Journal of Solid State Chemistry **166,** 426–433 (2002)
doi:10.1006/jssc.2002.9619

Study of Zircon–Dolomite Reactions Monitored by Neutron Thermodiffractometry

José Luis Rodríguez,*,[1] Antonio H. De Aza,*,[2] Pilar Pena,* Javier Campo,† Pierre Convert,† and Xavier Turrillas‡,[3]

*Department of Ceramics, Instituto de Cerámica y Vidrio, C.S.I.C., Antigua Ctra. De Valencia Km. 24.3 Arganda del Rey, 28500 Madrid, Spain; †Institut Laue-Langevin, 38042 Grenoble, France; and ‡Instituto de Ciencias de la Construcción Eduardo Torroja, C.S.I.C., 28032 Madrid, Spain

Received November 5, 2001; in revised form February 4, 2002; accepted April 19, 2002

The reaction mechanism that takes place in $ZrSiO_4$–$MgCa(CO_3)_2$ mixtures was studied in air up to 1300°C by collecting neutron diffraction patterns during the heating ramp. Neutron diffraction intensities were used to monitor and establish the mechanism of reaction that occurs in successive stages. (a) $MgCa(CO_3)_2$ decomposition yielding MgO and $CaCO_3$; (b) $CaCO_3$ decomposition; (c) reactions between CaO, MgO, and $ZrSiO_4$ involving the formation of phases such as: tetragonal-ZrO_2, α-Ca_2SiO_4, and $Ca_3MgSi_2O_8$, some of them acting as transitory phases; and (d) formation of $CaZrO_3$. The results obtained by this technique agree with data obtained by differential thermal analysis and thermogravimetry. The final product has a porous structure, due to the release of CO_2, with a very narrow pore size distribution ($\approx 1\,\mu m$). This open-porosity can be controlled by tailoring the reaction sintering process.

Key Words: **neutron thermodiffractometry; solid-state reactions; $MgCa(CO_3)_2$; $ZrSiO_4$; porous ceramics.**

INTRODUCTION

Porous ceramics with interconnected porosity and controlled pore size in the range of micrometers can be used to produce fluid-flow filters (industrial wastes, beverages, etc), light- weight structural components, high-temperature insulators or membrane supports (1, 2).

The preparation of materials with controlled microstructure and high porosity by a reaction sintering process between mixtures of raw materials with at least one of the components being a carbonate, offers the option of obtaining porous ceramic materials that can work at high temperature by a very cost-effective process (3, 4). To exploit this option, two minerals, dolomite ($MgCa(CO_3)_2$) and zircon ($ZrSiO_4$) were selected to produce MgO–$CaZrO_3$ based materials according to the following reactions:

$$ZrSiO_4 + 3MgCa(CO_3)_2 \rightarrow 3MgO + CaZrO_3 + \alpha - Ca_2SiO_4 + 6CO_{2(g)}, \quad [1]$$

$$2ZrSiO_4 + 5MgCa(CO_3)_2 \rightarrow 4MgO + 2CaZrO_3 + Ca_3MgSi_2O_8 + 10CO_{2(g)}. \quad [2]$$

During the reaction sintering process, two main phenomena occur: Porosity removal, by reducing the surface area (and thus energy) of the pores, and reaction. Consequently, it may be possible to tailor the microstructure (and therefore the pore size and distribution) by controlling the reaction sintering mechanism to produce ceramic materials with the desired properties.

Furthermore, to get a deeper insight on the way these processes occur, it would be very useful to follow those processes in real time with the help of a non-interfering technique. Since the main phases present are crystalline, diffraction techniques are the obvious choice, but in this case, a powerful and penetrating radiation would be necessary, i.e., either synchrotron light or neutron radiation. More precisely, the use of powder neutron diffraction allows collecting data at an adequate pace to get an acceptable time resolution. The advantage of this technique is that *in situ* recording of diffraction patterns permits the detection of transient phases, which otherwise cannot be detected by quenching and conventional diffraction methods.

Another important advantage of using neutrons—related to their penetration power—is the simplification of the ancillary setup. Indeed, furnaces of different types and other devices can be easily implemented. Furthermore, relatively bulky specimens, of a few centimeters length can be analyzed; and as the diffracting volume of the samples

[1] On leave CINVESTAV-IPN. Carr. Saltillo Coah., México.
[2] To whom correspondence should be addressed. Fax: +34 91 870 0550. E-mail: aaza@icv.csic.es.
[3] Also at ESRF, 38043 Grenoble, France.

0022-4596/02 $35.00

examined is rather large, the information collected is statistically representative of the whole.

Some recent examples where combined neutron diffraction with a high-temperature furnace used to study thermal decomposition reactions and phase transitions can be found elsewhere (5–8).

In the present investigation, the results obtained using time-resolved neutron diffraction methods to investigate the sintering process and the reactions that takes place up to 1300°C of different $ZrSiO_4$–$MgCa(CO_3)_2$ mixtures are discussed. The materials obtained have an homogeneous and narrow pore size distribution ($\sim 1\,\mu m$) with a porosity up to 40 vol.%.

EXPERIMENTAL PROCEDURES

The raw materials used in this investigation were as follows. $ZrSiO_4$ (Zircosil, Cookson Ltd), the main impurities being HfO_2 (0.1 wt%) and Y_2O_3 (0.11 wt%). This material has an average particle size of 1.23 μm (by laser diffraction) and a surface area of $12\,m^2/g$ (by B.E.T.). A finely milled mineral $MgCa(CO_3)_2$ supplied by Prodomasa, Spain, was used for this work. The composition, by weight, of main elements expressed as oxides is 30.29% CaO and 22.05% MgO. The main impurities as oxides are 0.018 wt.% SiO_2 and 0.011 wt.% Al_2O_3. This material has an average particle size of 4.9 μm (by laser diffraction) and a surface area of $2.5\,m^2/g$ (by B.E.T.)

Two $ZrSiO_4/MgCa(CO_3)_2$ compositions were prepared according to the stoichiometry proportions of Eqs. [1] and [2]. They will be referred along this paper as S2 and S4, respectively. By looking at the quaternary system CaO–MgO–ZrO_2–SiO_2 (9) it can be seen that their initial liquid formations start at 1750°C and at 1550°C, which are the invariant points of the MgO–$CaZrO_3$–Ca_2SiO_4 and MgO–$CaZrO_3$–$Ca_3MgSi_2O_8$ subsystems, respectively.

The $MgCa(CO_3)_2/ZrSiO_4$ mixtures were homogenized by attrition milling in water media. After spray drying, bars of about 5 mm diameter were pressed by cold isostatic press at 100 MPa. Details of the experimental procedure can be found elsewhere (3, 4).

Differential thermal analysis (DTA) and thermogravimetric analysis TG (STA 409, Netzch, Germany) studies were conducted on cold isostatically pressed compacts, in air, using Pt crucibles. The thermal studies were performed up to 1500°C and at a constant heating rate of 2°C/min.

Microstructural analyses and phase identification were done by scanning electron microscopy (Zeiss DMS 950, Germany) with energy dispersive X-ray analyzer using sputtered gold coating on fractured surfaces of the heat-treated samples.

The pore morphology was characterized by mercury porosimetry (model Autopore II 9215, Micromeritics Instrument Corp., Norcross, GA, USA). For these measurements, the pressure was increased up to 414 MPa in 126 steps (the final pressure corresponded to a pore diameter of 3.2 nm). At each step, the pressure was kept almost constant and held for 5 s.

Neutron Thermodiffractometry

The high-temperature neutron diffraction experiments were performed at Institute Laue-Langevin (ILL), Grenoble, France, in the instrument D1B ($\lambda = 2.52$ Å). Technical details can be found elsewhere (10).

An ellipsoid mirror furnace manufactured at ILL based in an initial design by Lorenz et al. (11) was placed in the diffractometer. Diffraction experiments were carried out by heating the samples from room temperature to 700°C, at a constant heating rate of 10°C/min, and then the temperature was raised to 1300°C at a rate of 2°C/min. Temperatures from Pt/Pt–Rd10% thermocouples were recorded continuously while diffraction data were accumulated every 150 s during the whole experiment.

The compacted specimens were placed into platinum crucibles of 5 mm diameter and 8 mm height, covered with a platinum lid to ensure an uniform heat distribution in the whole sample. A hole on the sidewall of the crucible allowed introducing another thermocouple to the center of the specimen.

Data Analysis

Data treatment details have already been described in a previous paper (6). General plotting was carried out with the help of commercial package Origin (12). The visualization of data in the form of three-dimensional (3D) plots and contour maps was made with the help of a commercial package, NOESYS (13). To measure inte-

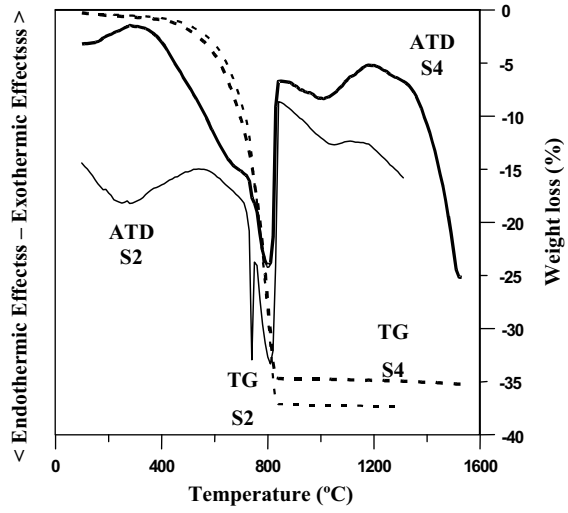

FIG. 1. DTA and TG of the two $MgCa(CO_3)_2/ZrSiO_4$ studied samples: S2 and S4.

grated intensities, reflections were fitted to Gaussian curves with procedures written in IDL (14).

Thermodynamic calculations, related to the free energy of reactions, were performed by using the Outokumpu HSC Chemistry computation package (Version 1.10) (15). The HSC offers an extensive thermochemical database which contains enthalpy (H), entropy (S) and heat capacity (C) data for chemical compounds.

RESULTS

The differential thermal analysis plot of the two $MgCa(CO_3)_2/ZrSiO_4$ studied samples, S2 and S4, are shown in Fig. 1. Both samples show significant weight losses of 37 and 35 wt.%, respectively, due to the release of CO_2. The two thermograms exhibit two endotherms, one at $\sim$745°C and the second at $\sim$800°C due to the $MgCa(CO_3)_2$ decarbonation in two stages at low CO_2 pressure (atmospheric pressure): $MgCa(CO_3)_2$ decomposition gives calcite ($CaCO_3$) and periclase (MgO) in a first step, and calcite breakup in a second step. These results are in agreement with those reported by Otsuka (16) and De Aza *et al.* (6). Both samples also show a broad exothermic effect at about 1150°C.

Thermodiffractometry

The diffraction data collected during the heating cycle were represented as a sequence of patterns in a pseudo-3D fashion in which the x-axis corresponds to the diffraction angle 2θ, the y-axis to the temperature and the z-axis to the relative intensity. The evolution in real time of the $MgCa(CO_3)_2/ZrSiO_4$ reactions of S2 and S4 compositions can be seen in the 3D diagrams of Figs. 2a and 3a.

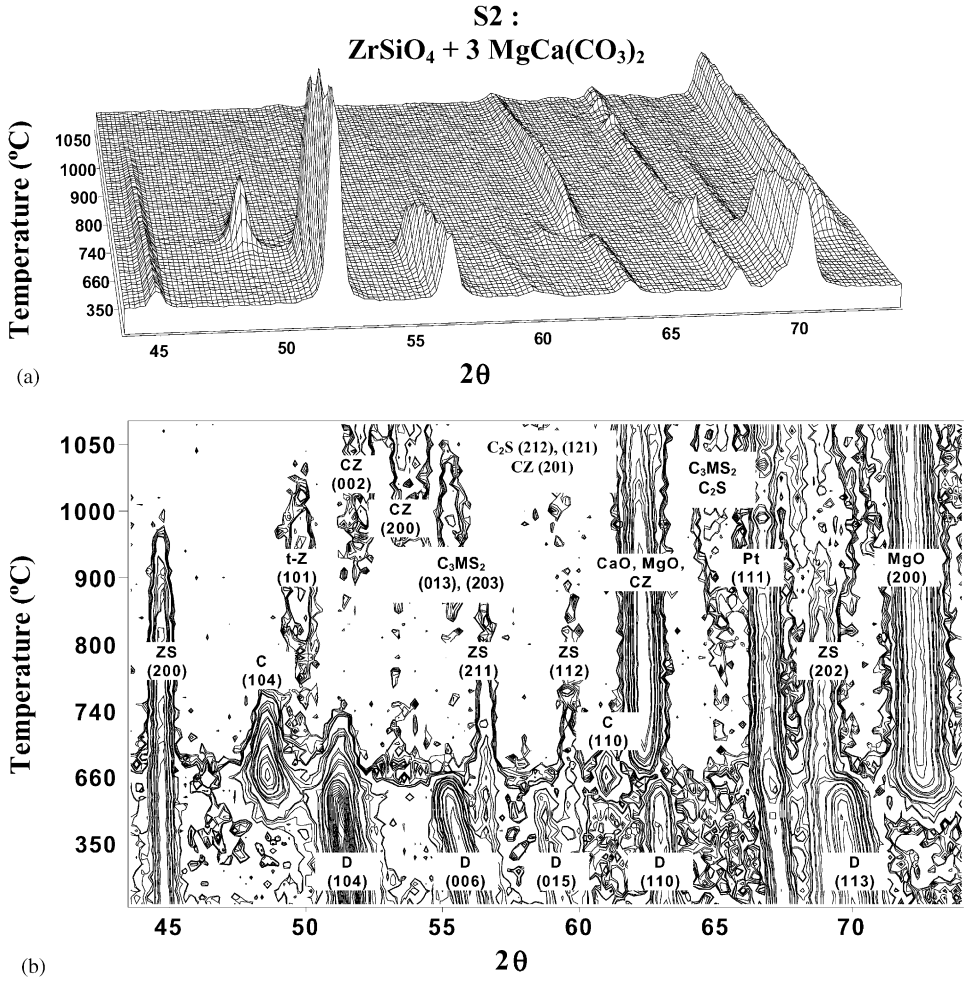

FIG. 2. (a) Sequence of powder neutron diffraction patterns for $3MgCa(CO_3)_2/ZrSiO_4$ mixture (S2) as a function of temperature. The corresponding Miller indices are indicated for the different phases. (b) Smoothed 2D contour projection of the 3D sequential map. For simplicity, phases given in the figures of this paper are described by abbreviated formulas. Notation used: D for $MgCa(CO_3)_2$, ZS for $ZrSiO_4$, C for $CaCO_3$, C_3MS_2 for $Ca_3MgSi_2O_8$, C_2S for α-Ca_2SiO_4, CZ for $CaZrO_3$, t-Z for tetragonal ZrO_2, Pt for platinum, CaO for lime, and MgO for magnesia.

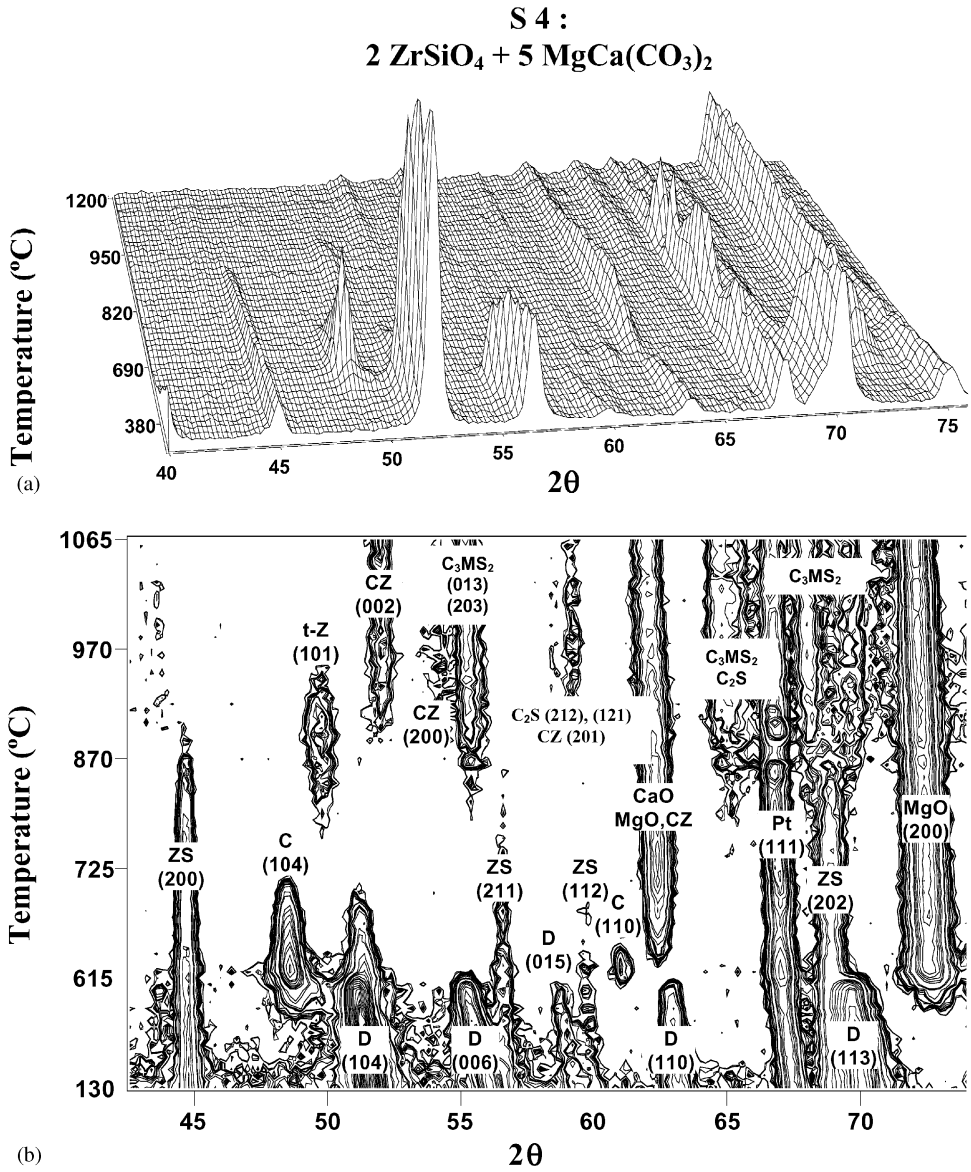

FIG. 3. (a) Sequence of powder neutron diffraction patterns for $5MgCa(CO_3)_2/2ZrSiO_4$ mixture (S4) versus temperature. Phases with their indexed peaks are highlighted. (b) Smoothed 2D contour projection obtained from the 3D sequential map. For the notation used, see caption of Fig. 2.

To visualize the events with more precision, the diffraction shifts and the collapse of phases, contour maps in two dimensions were also projected from the 3D plots (Figs. 2b and 3b). The phases domains of existence are highlighted by their diffraction peaks shown in the figures with the corresponding Miller indices.

The progress of reactions was followed by the integrated intensities of selected reflections, isolated from the rest, measured by fitting them to Gaussian curves as it has been explained before.

The variation of the integrated intensities of selected reflections for different phases as a function of temperature can be seen in Figs. 4a and 4b. These integrated intensities were normalized to 100. The plots stand out the progress of the reactions that takes place, i.e., the formation or the decay of a particular phase is related to the variation of the integrated intensities plotted.

The contour maps of Figs. 2b and 3b clearly show that $ZrSiO_4$ presence does not affect the $MgCa(CO_3)_2$ decomposition. Calcium carbonate appears at $\approx 550^{\circ}C$ and decomposes at $\approx 800^{\circ}C$ to yield CaO. The generation of MgO from the decomposition of $MgCa(CO_3)_2$ is also clear. These results are in agreement with previous studies of $MgCa(CO_3)_2$ decomposition by thermodiffractometry (6) and differential thermal analyses already mentioned (Fig. 1).

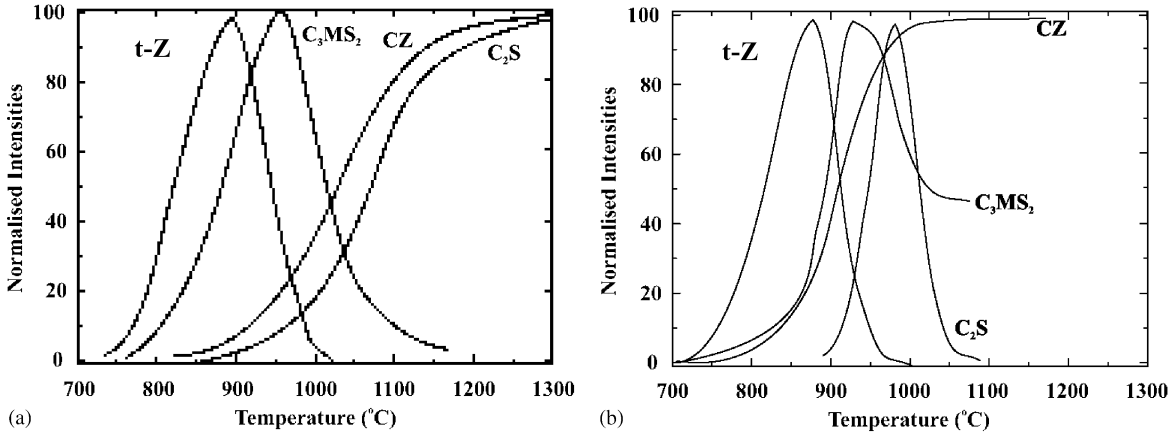

FIG. 4. Evolution of the crystalline phases during the reactions for (a) $3MgCa(CO_3)_2/ZrSiO_4$ mixture (S2) and (b) $5MgCa(CO_3)_2/2ZrSiO_4$ mixture (S4). Selected integrated intensities plotted versus temperature for reflections (1 0 1) of t-ZrO_2 (t-Z), (0 1 3) of $Ca_3MgSi_2O_8$ (C_3MS_2), (2 0 0) of α-Ca_2SiO_4 (C_2S), and (1 0 1) of $CaZrO_3$ (CZ).

By looking at Fig. 2b, it is clear that MgO diffraction peaks onset at 550°C and at 750°C they reach a maximum. This phase exists until the end of the registered temperature. At about 850°C, the first formation of $CaZrO_3$ (calcium zirconate) takes place and around 900°C that of α-Ca_2SiO_4. In the range 800–1200°C, the formation and collapse of two transitory phases are detected (t-ZrO_2 (tetragonal zirconia) and $Ca_3MgSi_2O_8$ (merwinite)).

Likewise, the evolution of the reactions for the S4 composition can be seen in Figs. 3a and 3b. MgO starts to manifest its presence at ≈550°C and the corresponding diffraction peaks grow until ~750°C. t-ZrO_2 appears at ~750°C and collapses at about 950°C. Progressing in temperature, in the range 900–1100°C the formation and collapse of α-Ca_2SiO_4 is also detected. The MgO exists until the end of the registered temperature range. At about 750°C, the first formation of $CaZrO_3$ and $Ca_3MgSi_2O_8$ takes place.

Additionally, both samples show a relatively broad diffraction peak below 5° 2θ with a maximum between 600°C and 1200°C (see Figs. 5a and 5b). For both experiments, this peak is by far the strongest one compared to the rest of the peaks. Its shape seems to be Gaussian like, although the left branch is not clearly defined due to the interference of the beam stop.

These diffraction peaks for both samples are shown in Figs. 6a and 6b. The variations of intensities, for this low-angle region, were plotted versus temperature, jointly with thermogravimetric curves. In these figures, a coincidence between the loss of weight due to the release of CO_2 (37% and 35% by weight) and the sudden growth of the low-angle peak is clear. As it will be discussed later on, this low-angle peak is related to the development of small particles and pores inside the samples.

Figures 7a to 7d show the typical microstructure of the fractured surfaces of S2 and S4 specimens after being heat treated at 1550°C/2 h and 1350°C/2 h, respectively. Grains

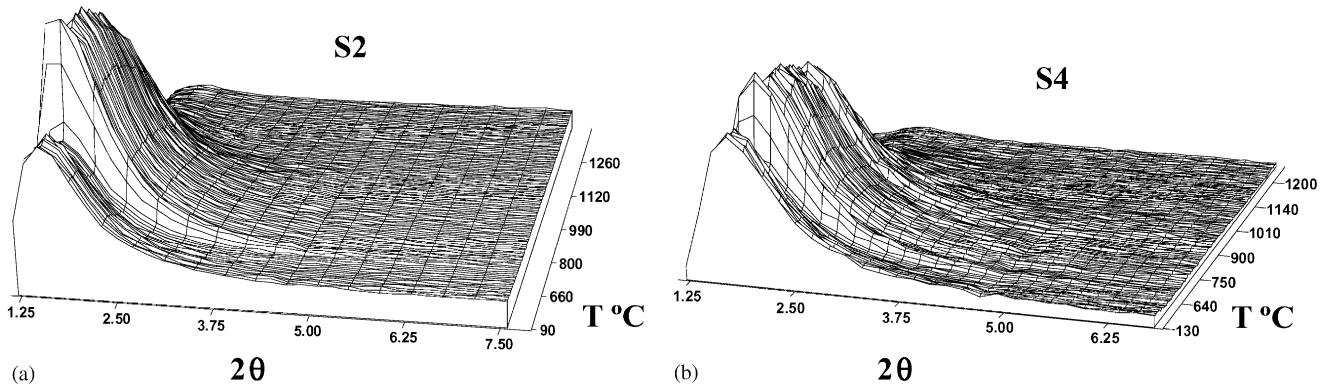

FIG. 5. Sequence of powder neutron diffraction patterns for the diffraction peak detected at the low angle region (below 5°, 2θ, versus temperature: (a) S2 sample and (b) S4 sample.

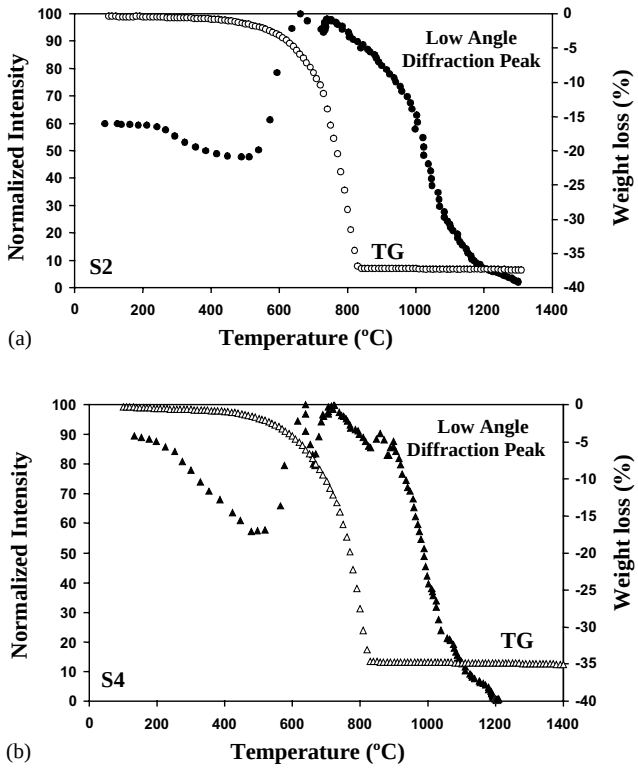

FIG. 6. Normalized integrated intensities for the diffraction peak detected at the low angle region, 1.2 – 5° (2θ) and TG versus temperature for (a) S2 sample and (b) S4 sample.

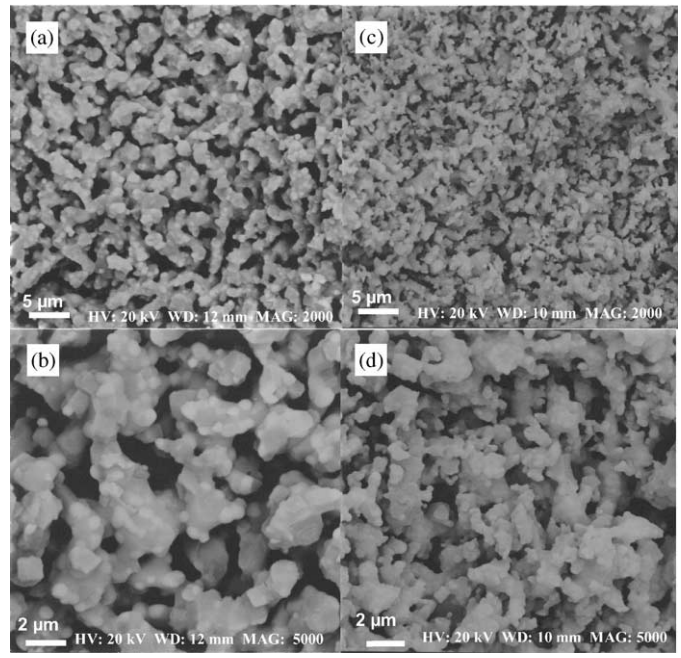

FIG. 7. (a)—(d) Typical microstructure of the fractured surfaces of the S2 (a–b) and S4 (c–d) composites sintered at 1550°C and 1350°C, respectively.

with bright contrast are $CaZrO_3$ and those with dark contrast are MgO or Ca_2SiO_4. Fig. 8 shows the pore size distribution of both samples. Both compositions show porous microstructures, ~40% porosity, with channels of interconnecting pores forming a well-developed 3D network structure (Table 1). The average pore diameter is ~1 μm and the grain size ~800 nm.

DISCUSSION

As it was observed in previous works (3, 4), the reaction sintering mechanism of $ZrSiO_4$–$MgCa(CO_3)_2$ mixtures occurs in two well-differentiated main steps: (a) reaction and (b) sintering of the reaction products. According to the high-temperature neutron diffraction data, the differential thermal analysis and the thermogravimetric examinations, here presented, during the heat treatment the $MgCa(CO_3)_2$ by-products (CaO + MgO) react with $ZrSiO_4$ (between 750°C and 1200°C) through a series of reactions before the final stable compounds are formed. Depending on the starting composition (either S2 or S4) the sequence of reaction is slightly different. Details of the thermal decomposition of $MgCa(CO_3)_2$ can be found elsewhere (6). In the present work, it can be seen that this decomposition is not altered by the presence of $ZrSiO_4$.

In the case of *the S2 sample*, the first crystalline phase observed after decomposition of $ZrSiO_4$ is t-ZrO_2, in agreement with the results obtained by Mursic *et al.* (7). These authors report that $ZrSiO_4$ dissociates at 1670°C. However, in the present work the $ZrSiO_4$ decomposition is observed at lower temperature due to the existence of CaO and MgO. It is obvious that $ZrSiO_4$ is not a stable phase in the presence of CaO + MgO above 700°C. From the data represented in Figs. 2 and 4a, the following reactions are

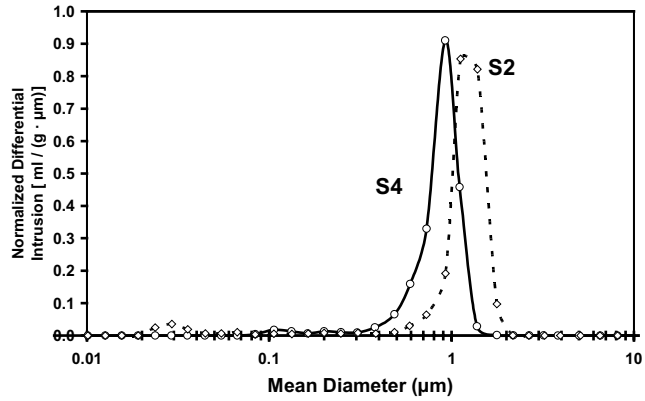

FIG. 8. Pore size distribution for both porous composites, S2 and S4, determined by mercury porosimetry.

TABLE 1
Pore Structure of the $MgO–CaZrO_3$ - Based Materials

Sample	Reaction sintering temperature (°C)	Mean pore size D (μm)	Porosity P(%)
S2	1250	0.77	60
	1350	1.03	51
	1550	1.14	40
	1740	—	1.4
S4	1250	0.72	42
	1350	0.83	41
	1450	0.78	21
	1550	—	4

Note. Both D (μm), mean pore diameter, and P (%), porosity, determined by mercury porosimetry.

proposed to interpret the observations:

$$CaO + MgO + ZrSiO_4 \rightarrow \textit{amorphous silica phase} + t - ZrO_2 \quad (775-1000^\circ C). \quad [3]$$

The *amorphous silica phase*, which cannot be detected by diffraction, reacts with CaO to form α-Ca_2SiO_4; stable phase that is present until the end of the experiment:

$$\textit{amorphous silica phase} + 2CaO \rightarrow \alpha - Ca_2SiO_4 \quad (T > 900^\circ C). \quad [4]$$

At temperatures higher than 775°C, t-ZrO_2 reacts with the remaining CaO to yield $CaZrO_3$, according to the following reaction:

$$t - ZrO_2 + CaO \rightarrow CaZrO_3 \quad (T > 775^\circ C). \quad [5]$$

A simultaneous process happens to form merwinite according to the reaction:

$$\textit{amorphous silica phase} + MgO + 3CaO \rightarrow Ca_3MgSi_2O_8 \quad (775-1100^\circ C). \quad [6]$$

The $ZrSiO_4$ decomposition, and the formation of α-Ca_2SiO_4 and $Ca_3MgSi_2O_8$ partially overlap and take place in a wide interval of temperatures ($\sim$775 – 1100°C). At higher temperatures, $Ca_3MgSi_2O_8$ reacts with the remaining CaO as follows:

$$Ca_3MgSi_2O_8 + CaO \rightarrow MgO + 2\alpha - Ca_2SiO_4 \quad (T > 900^\circ C). \quad [7]$$

Therefore, at the end of the process a mixture of $CaZrO_3$, α-Ca_2SiO_4, and MgO is present. On cooling, at approximately 630°C, the α-Ca_2SiO_4 phase transforms into the β-Ca_2SiO_4 phase, which is the one observed at room temperature. This is due to the small particle size of Ca_2SiO_4. According to (17), for particle sizes smaller than 5 μm, the polymorphic transformation β-$Ca_2SiO_4 \leftrightarrow \gamma$-$Ca_2SiO_4$ that takes place at approximately 500°C, accompanied by a volume expansion of 11% (that may produce a high density of microcracks in the material) does not occur.

In *the S4 composition* (Figs. 3 and 4b), the reaction path is similar, but here, $Ca_3MgSi_2O_8$ is the final stable phase whereas α-Ca_2SiO_4 is a transitory phase. The sequence of reactions is as follows:

$$CaO + MgO + ZrSiO_4 \rightarrow \textit{amorphous silica phase} + t\text{-}ZrO_2 \quad (T > 700^\circ C), \quad [8]$$

$$t - ZrO_2 + CaO \rightarrow CaZrO_3 \quad (T > 800^\circ C), \quad [9]$$

$$\textit{amorphous silica phase} + MgO + 3CaO \rightarrow Ca_3MgSi_2O_8 \quad (T > 800^\circ C), \quad [10]$$

$$\textit{amorphous silica phase} + 2CaO \rightarrow \alpha - Ca_2SiO_4 \quad (T > 900^\circ C), \quad [11]$$

$$2(\alpha - Ca_2SiO_4) + MgO \rightarrow Ca_3MgSi_2O_8 + CaO \quad (T > 980^\circ C). \quad [12]$$

At the end of the process, the phases present are $Ca_3MgSi_2O_8$, $CaZrO_3$, and MgO.

Thermodynamic calculations were used to support the detailed models of the reaction mechanisms. Table 2 shows these thermodynamic free-energy calculations for the reactions involved in both compositions (S2 and S4). It can be seen that the theoretical predictions agree with the sequential appearance of the phases. Let us provide here a concrete example of the convenience of these computations. The calculated ΔG for the formation of α-Ca_2SiO_4, $Ca_3MgSi_2O_8$, and $CaZrO_3$ confirm the much lower ΔG value for $Ca_3MgSi_2O_8$ formation, in the temperature region considered. Consequently, its appearance as the first phase during the reaction is clearly justified. The energy calculations (see Table 2) for reaction [7] ($\Delta G \sim$ 0 kcal/mol, also valid for [12]) indicate that in the 850 – 1100°C temperature range, α-Ca_2SiO_4 and $Ca_3MgSi_2O_8$ could coexist in equilibrium.

Concerning the microstructure of these materials, the formation of a porous structure built up by pores randomly

TABLE 2
Thermodynamic Calculations

Reaction	Reaction	$\Delta G_{(800–1100^\circ C)}$ (Kcal/mol)
Amorphous silica phase + 2CaO → α-Ca_2SiO_4	[4] [11]	– (33–34)
t-ZrO_2 + CaO → $CaZrO_3$	[5] [9]	–8
Amorphous silica phase + MgO + 3 CaO → $Ca_3MgSi_2O_8$	[10]	–62
$Ca_3MgSi_2O_8$ + CaO → MgO + 2 α-Ca_2SiO_4	[7] [12]	$\approx$0

Note. Performed using the HSC thermochemical database (15).

distributed in a solid skeleton of particles (<500 nm) can be followed in Figs. 5 and 6, as it was mentioned in the previous section. This low-angle diffraction peak is indeed related to the development of pores and small particles inside a homogeneous medium. Small angle scattering with both X-ray (SAXS) or neutron (SANS) are well-known techniques to study the distribution of different size particles inside a dominant phase. The instrument used for this work was not a dedicated SANS machine and obviously, precise parameters such as the pore size and/or distribution could not be quantified. However, it is possible to correlate in a rather qualitative way the development of the low-angle peak with the microstructural changes, namely the porosity. Therefore, the presence of this conspicuous peak is probably due to the submicroscopic porous structures formed by the thermal decomposition, of $MgCa(CO_3)_2$ and $CaCO_3$ (18) releasing CO_2. This fine porous structure is developed jointly with nano-particles of MgO and $CaCO_3$ in the temperature range 500–800°C. This phenomenon is observed in both compositions and the pores formed are responsible for the low apparent density of the final products.

Clearly, these ceramics have a high porosity and the mechanism of the porosity formation is related to the liberation of CO_2 during the decomposition of $MgCa(CO_3)_2$. The CO_2 gas liberated yields an homogeneous open-pore structure. According to SEM observations, both composites show a narrow pore-size distribution, with a mean size of $\sim 1\,\mu m$, which remain stable at temperatures as high as 1350°C and 1550°C for S4 and S2, respectively. These porous composites, $\approx 40\%$ of porosity, can be used as ceramic filters materials with a good structural stability at high temperatures or as insulating materials because of their low thermal conductivity, 1.5–0.7 $Wm^{-1}C^{-1}$ between room temperature and 800°C (19).

CONCLUSIONS

The preparation of materials with controlled microstructure and high porosity by a reaction sintering process of raw materials mixtures with at least one of the components being a carbonate, offers the option of obtaining porous ceramic materials that can work at high temperature. In this work, $CaZrO_3$–MgO-based composites with a porous structure were obtained by reaction sintering of highly pure mixtures of raw $MgCa(CO_3)_2$ and $ZrSiO_4$ powders. This method is very cost effective due to the use of natural raw materials and one-step heat treatment. The porous materials obtained can be used as filters with good structural stability at high temperatures and as insulating materials.

The reaction mechanism in $MgCa(CO_3)_2/ZrSiO_4$ mixtures up to 1300°C has been established by in situ neutron diffractometry. From the results obtained, it has been demonstrated that the reaction sintering occurs in successive stages. After the $MgCa(CO_3)_2$ decomposition into MgO and $CaCO_3$, in the 500–700°C temperature range, calcite breaks up to yield CaO at approximately 750°C. On further heating, from 750°C to 1050°C, CaO, MgO, and $ZrSiO_4$ react forming amorphous phases (silica-based phases), t-ZrO_2, $Ca_3MgSi_2O_8$, and α-Ca_2SiO_4. Some of these phases are only transitory phases and lead to the formation of $CaZrO_3$.

ACKNOWLEDGMENTS

This work has been possible thanks to beam-time allocated by the French–Spanish CRG of the Institute Laue — Langevin (ILL), France, experiment CRG-419. The authors wish to acknowledge financial support of the CICYT, Spain, under project number MAT - 2000–0941 and by CSIC/CONACYT cooperative project 99MX0023. J. L. Rodríguez wishes to acknowledge financial support from CONACYT (69147-Fellowship).

REFERENCES

1. N. Corbitt, "Inorganic Membranes: Markets, Technologies, Players." Business Communications Co., Inc., Norwalk, 1997.
2. K. Ishizaki, S. Kormarneni, and M. Nanko, "Porous Materials-Process Technology and Applications." Kluwer Academic Press, Dordrecht, Netherlands, 1998.
3. J. L. Rodríguez, M. A. Rodríguez, S. De Aza, and P. Pena, *J. Eur. Ceram. Soc.* **21,** 343–354 (2001).
4. J. L. Rodríguez, S. De Aza, and P. Pena, *Trans. Br. Ceram. Soc.* **100**(4), 181–191 (2001).
5. H. Yamane, M. Shimada, and B. A. Hunter, *J. Solid State Chem.* **141,** 466–474 (1998).
6. A. H. De Aza, M. A. Rodríguez, J. L. Rodríguez, S. De Aza, P. Pena, P. Convert, T. Hansen, and X. Turrillas, *J. Am. Ceram. Soc.* **85,** 881–888 (2002).
7. Z. Mursic, T. Vogt, H. Boysen, and F. Frey, *J. Appl. Crystallogr.* **25,** 519–523 (1992).
8. Z. Mursic, T. Vogt, and F. Frey, *Acta Crystallogr. B* **48,** 584–590 (1992).
9. S. De Aza, C. Richmond, and J. White. *Trans. J. Br. Ceram. Soc.* **73**(4), 109–116 (1974).
10. http://www.ill.fr/YellowBook/D1B/.
11. G. Lorenz, R. B. Neder, J. Marxreiter, F. Frey, and J. Schneider, *J. Appl. Crystallogr.* **26,** 632–635 (1993).
12. Program Origin Version 5.0. Microcal Software Inc. , Northampton, MA, USA.
13. Noesys version 1.2 © 1992–1998. Fortner Software LLC.
14. IDL version 5.2.1 (win 32×86) © 1999. Research system Inc.
15. "Outokumpu HSC Chemistry for Windows," Version 1.10. Outokumpu Research Oy, Pori, Finland, 1993.
16. R. Otsuka, *Thermochim. Acta* **100,** 69–80 (1986).
17. J. S. Moya, P. Pena, and S. De Aza, *J. Am. Ceram. Soc.* **68**(9), C-259–C-262 (1985).
18. D. R. Voller, J. A. Varela, *J. Am. Ceram Soc.* **74**(10), 2683–2685 (1991).
19. J. L. Rodríguez-Galicia, Ph.D. Thesis, Universidad Autónoma de Madrid, 2001. [In Spanish]